Space Science and Engineering Center
University of Wisconsin–Madison

A REPORT
OF THE
SEVERE WEATHER PROGRAM
FOR THE PERIOD
1 SEPTEMBER 1993 TO 31 AUGUST 1994

A REPORT from the

COOPERATIVE INSTITUTE FOR METEOROLOGICAL SATELLITE STUDIES

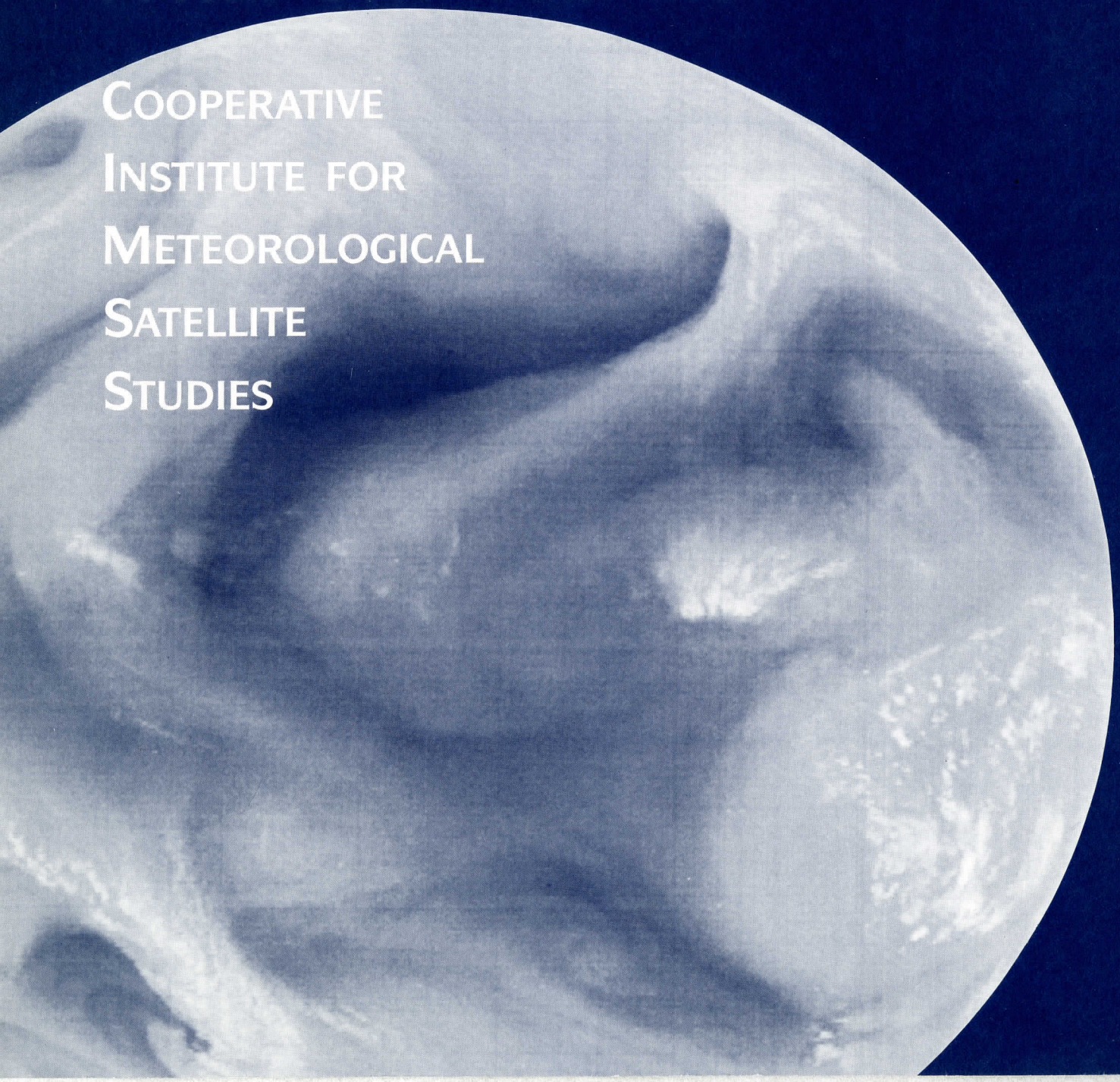

A REPORT
OF THE
SEVERE WEATHER PROGRAM
FOR THE PERIOD
1 SEPTEMBER 1993 TO 31 AUGUST 1994

Submitted by

Cooperative Institute for Meteorological Satellite Studies
Space Science and Engineering Center (SSEC)
at the University of Wisconsin-Madison
1225 West Dayton Street
Madison, Wisconsin 53706
(608) 263-7435

William L. Smith
Director, CIMSS
Principal Investigator

Anthony J. Schreiner
Associate Researcher
Program Manager

Christopher M. Hayden
Chief, SDAB
Principal Scientist

I. INTRODUCTION

II. RESULTS

A. Report on the Improvements to the CRAS Real-Time Forecast System and Assimilation of Satellite-Derived information. Contributed by Robert M. Aune.

B. Satellite data assimilation on the CIMSS Regional Assimilation System (CRAS). Contributed by Xiaohua Wu.

C. Development of a Verification Package to the CIMSS Regional Assimilation System (CRAS). Contributed by Mark Whipple.

D. Improved Precipitation Forecasts Using Parameterized Feedback in a Hydrostatic Forecast Model. Contributed by William H. Raymond and Robert M. Aune.

E. The Initialization of Moisture in Numerical Forecast Models. Contributed by William H. Raymond.

F. Upper Tropospheric Relative Humidity from Geostationary Satellite Water Vapor Radiance Data. Contributed by Xiangqian Wu.

G. GOES-8 derived imagery development and utilization of GALE VAS temperature/moisture retrievals. Contributed by Gary S. Wade and Robert M. Rabin.

H. Development of a Microburst Risk Image Product from Satellite Sounder Data. Contributed by James P. Nelson and Gary P. Ellrod.

I. Development of a Gridded Cloud Product from GOES-8 Radiance Data. Contributed by Anthony J. Schreiner and Christopher M. Hayden.

III. PERSONNEL AND EQUIPMENT

IV. SUMMARY

V. REFERENCES

I. INTRODUCTION

This annual report describes the work done during the final year of a three year funding period. The period covered is from 1 September 1993 through 31 August 1994. The scope of this report is twofold: first, to give a brief summary of the various and diverse projects being funded during the contract period (RESULTS); second, to denote the personnel supported and equipment acquisition needed to accomplish the goals detailed in section II (PERSONNEL AND EQUIPMENT). Sections IV and V summarize and list references, respectively. The reference section includes all published papers and conference reports resulting from this research work plus the cited articles in the Results section.

The three main research areas covered in the RESULTS section of this report are:

- The evolution and improvements of the CIMSS Regional Assimilation System (CRAS) model at CIMSS. Continued streamlining and additional applications are being developed for the CRAS. Five articles discuss this progress.
- The development of satellite-derived products using the VISSR Atmospheric Sounder (VAS) and the GOES-8 Sounder and Imager radiance information. Application of derived-products for the purpose of understanding and forecasting the weather, and to be used as input to numerical prediction models, continues to be an area of concentration. Three articles discuss the growth and evolution of these products for both the GOES-7 VAS and the GOES-8 remote sensors.
- Derivation of an image and gridded cloud product using the GOES-8 Sounder data. With the advent of the Global Energy and Water Cycle Experiment (GEWEX), there is a requirement for an hourly gridded cloud product over the continental United States. One article discusses the development of an algorithm which will satisfy this need.

II. RESULTS

A. Report on the Improvements to the CRAS Real-Time Forecast System and Assimilation of Satellite-Derived information. Contributed by Robert M. Aune.

1. The CRAS Real-Time Forecast System

The CIMSS Regional Assimilation System (CRAS) continues to produce real-time numerical weather predictions every 12 hours, along with experimental predictions that incorporate experimental data from weather satellites. Data impact studies were conducted using cloud track winds, water vapor winds, and total precipitable water from GOES-7. CRAS forecasts were also used operationally to support field programs such as the ARM Project's CARTE experiment in Oklahoma. In addition, real-time CRAS products are distributed for public viewing on the University of Wisconsin closed-circuit TV network and on the Space Science and Engineering Center's Gopher server.

Currently, there are two CRAS forecast systems producing real-time forecasts: Fine-mesh (60 km) and Coarse-mesh (150 km). Details of the forecast systems are presented in Table 1. The Coarse-mesh forecast continues to run on an IBM RS6000 Model 530. The Fine-mesh forecast was ported to a new SGI IRIS/CRIMSON which is faster and has improved visualization capabilities.

	Fine-mesh	Coarse-mesh
Type:	Semi-Implicit P.E., Non-hydrostatic	
Resolution; Horizontal (km):	60	150
Vertical levels (Sigma):	28	20
Grid size:	101x81	73x67
Time step (sec):	300	720
Forecast length (hours):	48	72
Output interval (hours):	3	6
Initial times (UTC):	00/12	00/12
Execution times (Local):	0200/1700	0230/1345
CPU time (min.):	270	120
Analysis guess:	CRAS 12 hour Fcst	NMC Aviation
Analysis input data:	RAOBS/AVHRR SST/SFC	
Verification data:	RAOB/SFC/ANALYSIS/SAT	
Current applications:	UW Looper	Boundary Conditions
	SSEC Gopher	Cloud Track Winds
	GOES-7 Cloud/vapor	H2O winds

Table 1. Current CRAS forecast configurations

As is the case with all numerical weather prediction systems, the CRAS is continually evolving. Numerous improvements in the Analysis, Pre-forecast, and Forecast modules were made in the past year. Significant improvements include:

1) A precipitation drag term was added to the equation for vertical motion used to compute the vertical advection of temperature. The term is parameterized as a function of condensed precipitation and the vertical motion itself, and is therefore self-limiting. Grid point storms due to unstable vertical motion/latent heat feedback were eliminated and affected areas of light precipitation remain unaffected.

2) A software package to statistically verify CRAS forecasts against surface and RAOB data was implemented. Verifications occur daily as part of each forecast cycle.

3) The fine mesh CRAS (60 km) analysis began using the previous 12 hour forecast as the background guess. The analysis was previously initialized using the NGM (190 km grid) analysis. This change reduced the spin-up time in the forecast.

4) A snow cover condition was added to the surface radiation parameterization. A snow cover analysis was introduced in the pre-forecast using surface snow-depth observations.

5) The surface skin temperature, formerly initialized with the lowest sigma-level air temperature, is now being initialized using observations of surface air temperature.

6) The CRAS analysis was modified to analyze 25 hPA layers up to the top (50 hPA) instead of 50 hPA layers up to 100 hPA This will resolve more detail near the surface and more accurately define the level of the tropopause.

2. Satellite Moisture Assimilation

The assimilation of moisture information concentrated mainly on how to use total precipitable water from VAS on the GOES-7 satellite. Numerous algorithms were tested resulting in an approach that adjusts the mean mixing ratio profile of the model to match the observed total precipitable water from VAS, while retaining the vertical distribution of the forecast. Thirty-four VAS and NOVAS forecasts were generated on random cases between August 1993 to June 1994. These VAS runs used the mean profile adjustment scheme with a correction to account for model surface elevation disparities (Aune 1994). Figure 1 shows the RMS difference of the VAS forecast verification minus the NOVAS verification. Of the 34 forecasts, only five cases showed significant positive impact, nine cases showed negative impact, while the rest showed little change. The cases that showed a positive impact generally involved systems in the Pacific moving onshore. The VAS data appears to have improved the moisture distribution in the vicinity of the storms. It is not clear what caused the negatively impacted cases. Weaknesses in the assimilation approach plus errors in the VAS retrievals are likely candidates.

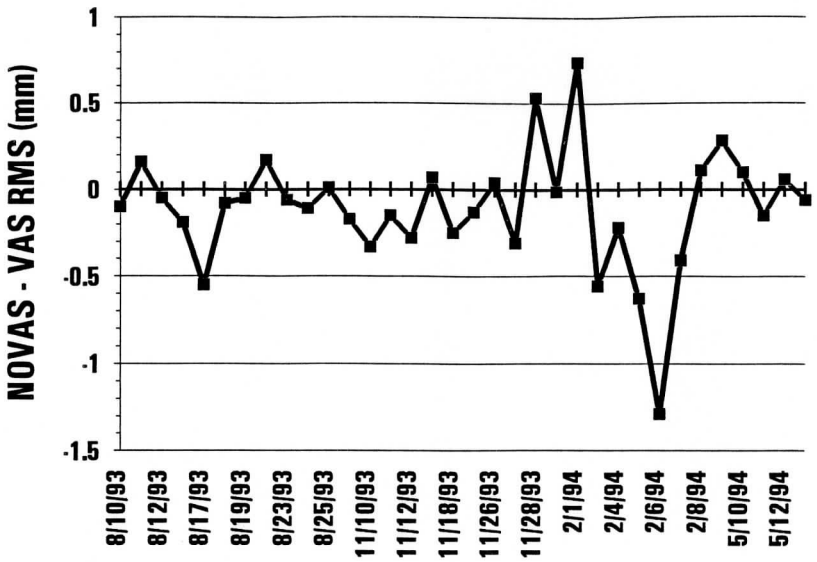

Figure 1. RMS comparison: NOVAS-VAS for 24 hour forecast precipitation verified against 24 hour accumulated precipitation from surface observations.

3. Satellite Wind Assimilation

The use of satellite wind information in the CRAS was investigated by the CRAS Assimilation Team (CAT). Three experiments were conducted using wind information derived from satellites.

1) Cloud Track Winds from METEOSAT. The initial conditions for 27 August 1993 containing hurricane Emily were analyzed using cloud track winds from METEOSAT. A 3D variational blend was used to adjust the mass fields to the momentum analysis. A convergent rotational bogus vortex with a supporting relative humidity field was inserted in the initial fields to represent hurricane Emily. A supporting anti-cyclonic circulation was introduced in the top layers below the tropopause. The model was able to maintain the vortex for 48 hours after a 12 hour nudge period. The METEOSAT wind data produced a significant improvement in the hurricane's 48 hour forecast track.

2) Water vapor winds from GOES-7 and METEOSAT. An experimental forecast was generated that assimilates cloud track winds from GOES-7 and METEOSAT every 12 hours for the month of March and part of April. The forecasts were produced using the 150 km CRAS. Data was assimilated using the 3D variational gradient blend option in the analysis. The CRAS control forecasts were set up to use the operational cloud track winds, VAS gradient winds, and ASDAR winds. The corresponding experimental forecasts incorporated the above-mentioned winds plus water vapor winds from GOES-7 and METEOSAT-3. Figure 2 shows the RMS differences of 72 hour forecasted 400 hPA heights for 52 cases, water vapor winds forecasts minus no water vapor winds. Of the 52 forecasts, 29 showed significant positive impact, 13 showed negative impact, while 10 showed little change. The cases that showed a positive impact generally involved systems moving over CONUS from data sparse areas. It is not clear what caused the negatively impacted cases. Weaknesses in the 3D variational blending approach may be at fault. Similar results were seen in the 24 hour, 36 hour, and 48 hour forecasts of heights at 700 hPA and 500 hPA.

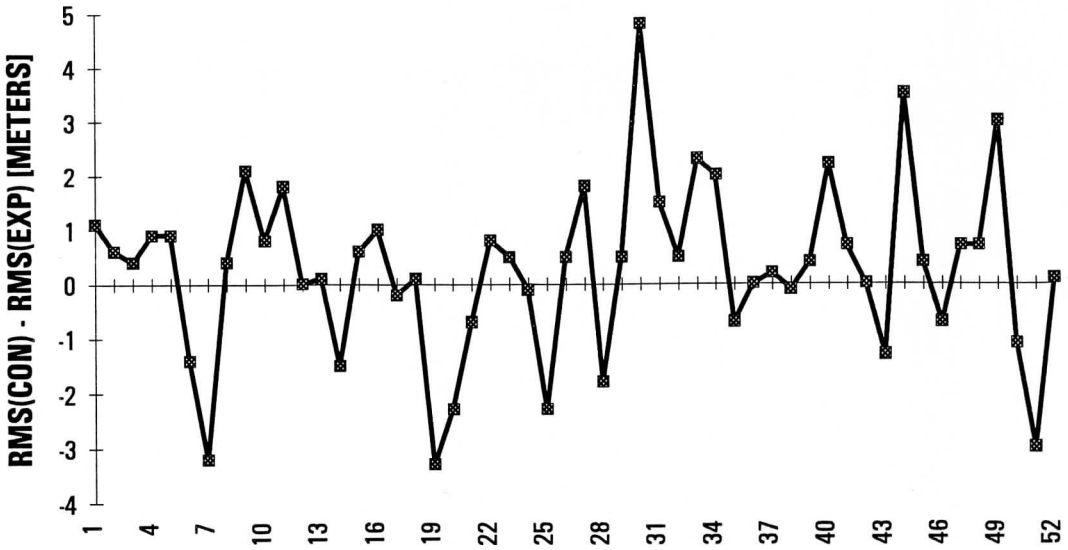

Figure 2. RMS differences of 72 hour forecasted 400 hPA heights verified against RAOBS for 52 cases, water vapor wind forecasts minus no water vapor wind forecasts. Positive numberr indicates improvement.

4. Four Dimensional Assimilation

To gain experience in 4D assimilation, a simple 3D (x,y,t) variational assimilation system was designed around a 2D barotropic model and its adjoint. The system uses code from the existing 2D shallow water system and analysis code from the CRAS interactive analysis system. The model is initialized with fields from the NMC's Northern Hemisphere Aviation analysis and is coupled with an advection equation to predict the movement of a passive parameter. The adjoint to the 2D barotropic model was derived. A software system to implement a 3D-VAR is still under development. Experiments will be conducted to study non-linear error growth and forecast model sensitivity to observation errors.

B. Satellite data assimilation on the CIMSS Regional Assimilation Model (CRAS). Contributed by Xiaohua Wu.

1. Short-Range Precipitation Forecasts Using Assimilation of Simulated HIRS-AMSU Water Vapor Profiles and Cloud Liquid Water

The principal emphasis of this study is on the assimilation of satellite-observed water vapor and cloud liquid water data in the initialization of a limited-area primitive equation model in order to improve short-range precipitation forecasts. The assimilation procedure presented includes two critical aspects: specification of a initial cloud liquid water distribution and diabatic initialization.

A diagnostic method to specify an initial cloud water distribution is presented, based on satellite-observed cloud-top height and total column cloud liquid water amount. This method diagnoses the existing clouds, modifies the initial moisture distribution in cloudy areas and specifies the cloud water distribution. Using this diagnostic cloud water method in conjunction with diabatic initialization, latent heating profiles are then directly assimilated into the numerical model. The estimate of diabatic heating rates are obtained by time averaging the latent heat release from convective and large-scale condensation during the early forecast stage after insertion of satellite-observed temperature, water vapor and cloud water information.

The dynamic balance induced by the diabatic initialization reaffirms the conclusion that adiabatic initialization is unable to generate divergent circulations which are diabatically driven. With large-scale latent heating rates, diabatic initialization can generate divergent circulations which are consistent with the cloud field's latent heating sources. The experimental forecasts emphasize that the short range precipitation problem cannot be solved by diabatic initialization alone; improvement of the initial moisture distribution by incorporating new data is critical.

The assimilation of satellite-observed moisture and cloud water together with diabatic initialization significantly reduces the precipitation spin up problem, especially in the earliest three hours, because of the ability to improve the initial moisture distribution and diagnose the existing clouds and specify associated circulations. The experimental forecasts indicate that the impact of satellite-observed temperature, water vapor and cloud water alone shortens the spin up time of precipitation rates by one to two hours and of areal coverage by three hours. Diabatic initialization together with cloud water initialization further reduces the precipitation spin up time (compared to adiabatic initialization) by one hour.

2. Variational assimilation of VAS-observed gradient wind data into the CRAS

A recurring problem with satellite-retrieved temperature is systematic error or bias. To avoid the data bias problem, the aim of this research has focused on assimilating VAS gradient wind information into the CRAS because satellite-observed gradient information may be more reliable than the absolute

values. To avoid the unduly large growth of gravity waves by suddenly inserting satellite data into NWP, a variational assimilation technique is used.

2.1 The impact of VAS gradient wind on the CRAS

The effort of this work is to investigate the impact of VAS gradient wind on the CIMSS Regional Assimilation Model (CRAS) numerical weather forecasts, especially in data sparse areas like the Northern Hemisphere ocean areas. The VAS wind data used in this investigation was collected during May and June 1994. The impact of VAS gradient wind on NWP is assessed in daily 12-hour numerical forecast experiments.

The model forecasts are performed on a twenty-level, 150-km mesh over an area represented by 73x53 grid points on a Lambert conformal projection, with standard latitude at 20 °N and 50 °N. The daily numerical forecast is run from 0000 UTC to 1200 UTC. VAS gradient wind produced at 0000 UTC of each day, covering the latitude extent 23 - 49 °N, is spread over a 550 hPA depth (from 850 to 300 hPA) by linearly interpolating the VAS data into the 50 hPA interval pressure levels and is incorporated into the initial fields of the 12-hour forecast through the data analysis procedure. The impact of the VAS gradient wind is investigated by the comparisons of forecasts started from four different analyses. The background fields for the analyses are obtained through interpolation of the NMC global (aviation) 12-hour forecast (from -1200 UTC to 0000 UTC) to the CRAS grids.

Analysis I incorporates just the conventional radiosonde-observed synoptic data (RAOB) at 0000 UTC, is used to emulate operational. Analysis II combines the RAOB with the VAS gradient wind in the background fields. The influence of the VAS wind to the model initial mass field (i.e., geopotential height and temperature) is obtained through the variational 'field information blending' (FIB) technique (Seaman et al. 1977), in which geopotential gradient is obtained by using observed VAS wind components via the geostrophic assumption. Analysis III incorporates the VAS wind data into wind component analysis only and omits variational FIB. Analysis IV keeps the impact of VAS gradient wind in mass fields only (i.e., the satellite wind is only used in the FIB procedure), and incorporates only RAOB data in the initial wind field.

The results obtained from these NWP experiments have indicated the significant impacts of VAS gradient wind in SSM forecasts compared with the conventional forecasts. Large differences in the analyzed temperature (T) and wind (U and V) fields have been found after incorporating VAS gradient wind data in analysis II. The mean maximum DT reaches 2 °K and can be 10 m/s in DU or DV fields. In Pacific Ocean areas, the differences are significant. Those DT, DU and DV distributions were mostly retained during the 12-hour forecasts starting from the analysis II. The forecast results also indicated that the initial mass fields must be consistently balanced with the wind fields. When VAS wind data were applied to wind component analysis only (analysis III), the forecasts showed that the intensity of DU and DV centers became smaller compared to the forecasts starting from analysis II. Furthermore, DT became

significant compared to the conventional forecast, even though the initial T fields were exactly the same in these two forecasts. This is the result of mass field adjustment to the initial wind fields. When the VAS wind data was only used in the f blending procedure (analysis IV) (i.e., the initial U and V fields were exactly the same to those in the analysis I), the forecasts showed that the initial DT, with smaller scale distribution, gradually diminished during the first six hours forecast. This fact implies that for lack of consisted VAS wind component analyses, DT caused by the f field blending with VAS wind cannot be retained during a 12-hour NWP because of the quick geostrophic adjustment of mass to the initial wind field. In the same time, DU and DV occurred as the results of wind fields adjusted to the initial DT distribution. These NWP experiments suggest that variational FIB is able to obtain initial mass information by incorporating VAS gradient wind information into the blending procedure. The ability and the accuracy of the variational FIB to exploit the gradient wind information inherent in geopotential height and temperature data fields, therefore, must be tested further.

2.2 Testing variational FIB to exploit the gradient wind information inherent in geopotential height and temperature fields

Since the impact of satellite data assimilation on NWP is dependent on the quantity of data available and the method used to assimilate the data, this work focuses on testing the ability and accuracy of variational FIB method to exploit the geopotential gradient information inherent in wind fields. The tests are focused on model simulations.

First, a set of 'observed'-wind data is extracted from the wind fields produced by the SSM 12-hour forecast at 50 hPA pressure levels and every two grid points (300 km in both x and y directions). For the purpose of the test, the CRAS forecast wind and temperature fields are considered to be the "truth". The first guess fields used for the analysis are obtained from the NMC's global model 12-hour forecast. The 'observed'-wind data is incorporated into the variational FIB procedure by translating the wind data to the geopotential gradient. The constraint used in FIB is to match the gradient data and the model first-guess absolute value. Finally, the analyzed temperature (or geopotential height) fields obtained from the variational FIB are compared with the 'truth' temperature fields at each pressure level.

The comparisons between the analyzed temperature and the 'truth' indicated that the variational FIB technique used in CRAS can extract the important structure distribution in mass fields through incorporating wind data into the variational blending procedure. However, the accuracy of the blended temperature or geopotential height is less. It may be caused by lower boundary in the forecast domain.

C. Development of a Verification Package to the CIMSS Regional Assimilation System (CRAS). Contributed by Mark Whipple.

One of the most fundamental questions that a numerical weather modeller can ask himself is, "Is my model's forecast correct?" To address this concern at CIMSS, A model verification package to be used with both our Coarse (150 km horizontal resolution, 20 vertical levels, 72-hour duration) and Fine (60 km horizontal resolution, 28 vertical levels, 48-hour duration) mesh model runs was developed. The verification software is designed to be clock-activated once the 12 UTC or 00 UTC model run is complete.

Three types of verifications are available to be performed: verification against gridded data, verification against RAOB data, and verification against surface observations. Any combination of these three verification types can be selected by simply modifying a table which the UNIX clock scheduler periodically scans for activities to perform. Each verification type is controlled by an associated run deck that determines which variable type and pressure levels are to be verified. Therefore, in order to change the type of verification being performed, one must only change the run deck.

The grid to grid verification program is intended to verify model predicted quantities at a given level against an analysis grid at the same time and level. This procedure is repeated for each 12-hour forecast interval until all forecast data sets have been verified against an analysis grid. For instance, the Fine-mesh model will have its 0, 12, 24, 36, and 48-hour forecast data sets verified against analysis data sets as these verification times come to pass. Each level and quantity verification will produce forecast mean, analysis mean, RMS error, and bias statistical quantities. The verification against radiosondes proceeds in a similar fashion, except that vertical profiles are extracted from model data sets and compared to RAOB quantities. The capability exists to verify both analysis and forecast data sets against radiosondes. Finally, surface quantities produced by the CRAS model may be verified against surface observations. Currently, surface pressure, model skin temperature, model skin dew point temperature, the surface wind components, and 6 and 24-hour predicted precipitation are being verified.

In order to visualize the statistical quantities, software was developed to generate a time series plot of data using the output data sets produced by the verification package. The file containing the time series could then be displayed using the share ware on the RS6000 workstation.

D. Improved Precipitation Forecasts Using Parameterized Feedbacks in a Hydrostatic Forecast Model. Contributed by William H. Raymond and Robert M. Aune.

Summary

An empirical parameterization of the non-hydrostatic mechanisms of precipitation drag and small-scale diabatically-induced mixing is introduced into a hydrostatic regional forecast model to curb excessive grid scale precipitation production. The non-hydrostatic vertical acceleration is equated to a Rayleigh damping term which allows the damping contributions to be easily incorporated into the forecast model using a modified version of the quasi-hydrostatic approximation (Orlanski 1981). The Rayleigh damping coefficient is set proportional to the predicted amount of liquid water. Two precipitation events are examined in detail, while statistics for several other forecasts are also presented. In our study, forecasts using the new parameterization are compared to those produced using horizontal diffusion and with actual precipitation observations. It is found that heavy precipitation production is significantly reduced by the parameterization, while periods of light precipitation are not impacted.

Illustration

The proposed drag and diabatic mixing parameterization is tested in detail using the CIMSS Regional Assimilation System (CRAS) forecast model. For illustration purposes, results from a 48 hour forecast beginning at 1200 UTC 12 March 1993, covering part of the time period during of the Great Blizzard of 93, are presented. The accuracy of the control forecast (no parameterization) is illustrated in the scatter diagram shown in Figure 1a, which compares the forecasted precipitation (ordinate) with precipitation observations (abscissa). When the drag parameterization is used the corresponding precipitation forecast is improved and the large amount of scatter found in Figure 1a is significantly reduced as shown in Figure 1b.

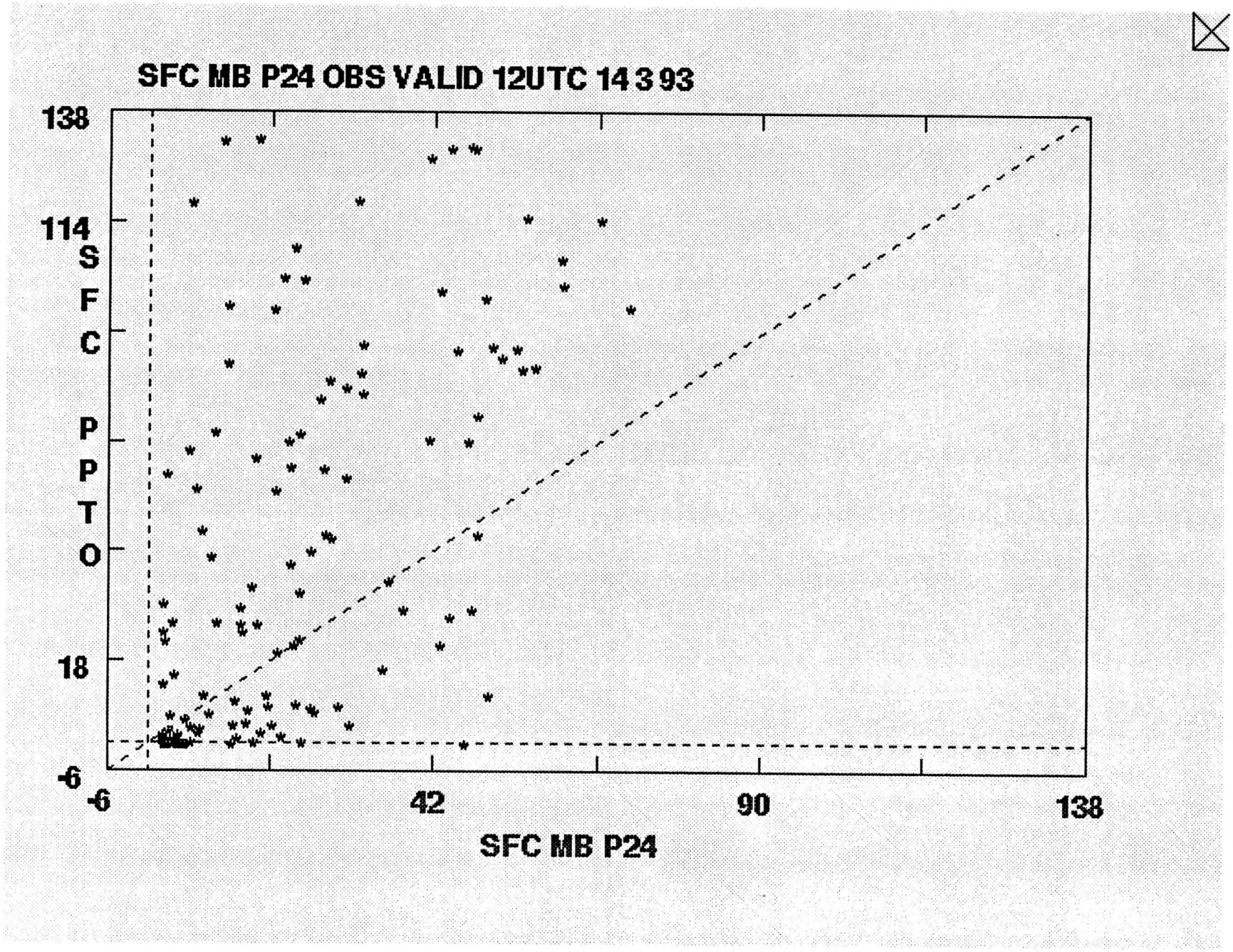
SFC MB P24 OBS VALID 12UTC 14 3 93
138
114
18
-6
SFC PPTO
-6
42
90
138
SFC MB P24

Fig 1a

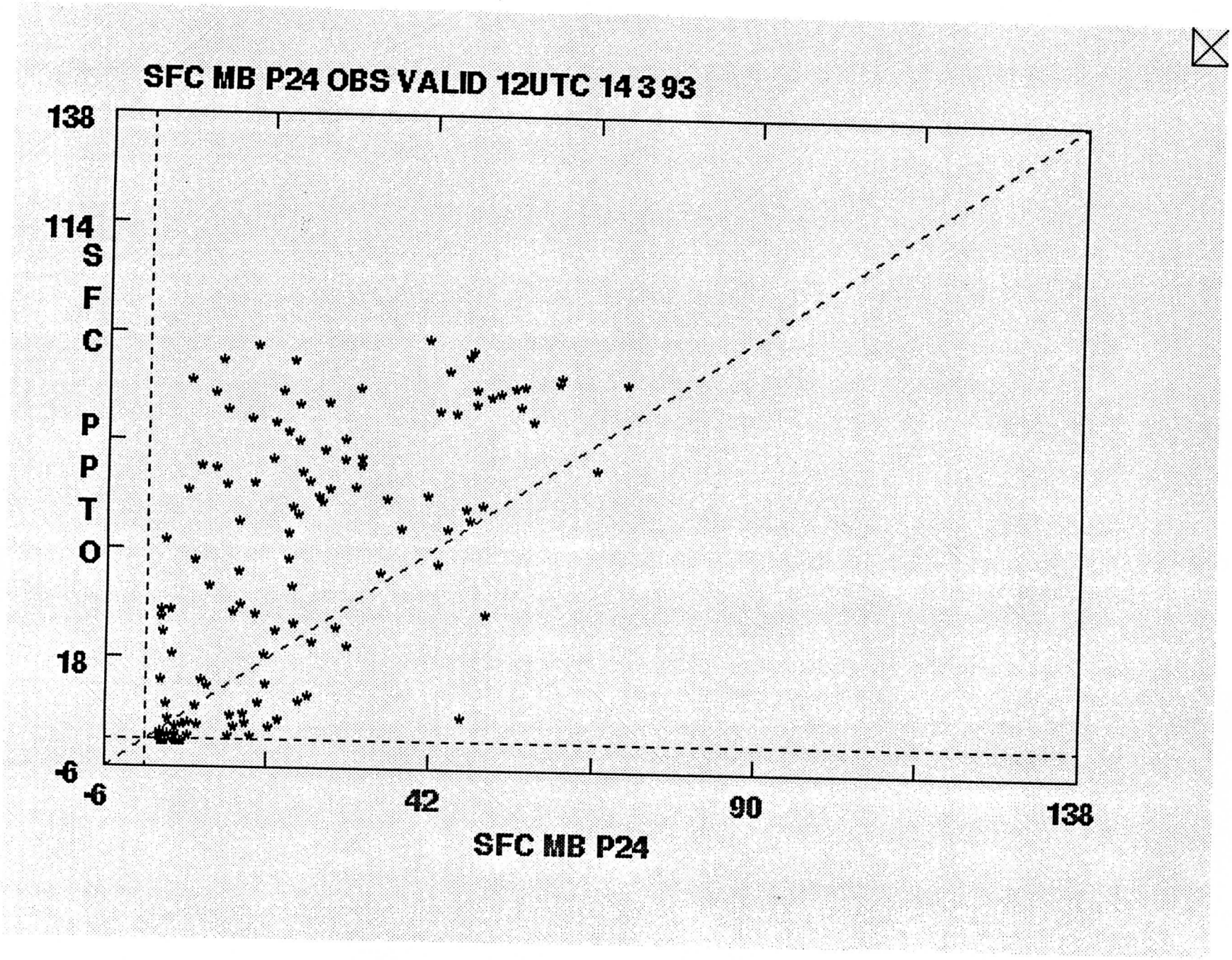
SFC MB P24 OBS VALID 12UTC 14 3 93
138
114
S
F
C
P
P
T
O
18
-6
-6
42
90
138
SFC MB P24

91 64

E. The Initialization of Moisture in Numerical Forecast Models. Contributed by William H. Raymond

Summary

There is not yet a satisfactory method to initialize the mixing ratio field for numerical models. Furthermore, the lack of a balance condition for the mixing ratio enhances the difficulty of distributing in the vertical the information contained in satellite observations of the total precipitable water. In this study a mathematical shooting technique is combined with a variational procedure, so that a specified total precipitable water is obtained while at the same time constraining the vertical profile of the mixing ratio to be variationally in balance with the governing partial differential equation.

Discussion

Water vapor is not included in the normal mode or vertical mode initialization techniques used by modellers to balance the atmospheric dynamics with the mass field. In fact, modellers lack any "balance" equation to assist them in the initialization of the mixing ratio field. Nevertheless, some manipulation or modification of the water vapor field is required to resolve differences between model predictions and satellite observational measurements. This is especially critical in the vertical coordinate because of the rapid change of the mixing ratio with height. In our study, we have identified a mathematical shooting method that allows us to reproduce the total precipitable water field, and at the same time impose the constraint that the variational solution be consistent with the partial differential equation governing the mixing ratio. These calculations require knowledge of the vertical motion ω and require the solution of a second order elliptic equation.

Vertical motion either enhances or suppresses the vertical transport of moisture depending upon the sign of the vertical velocity ω (pressure coordinate). The importance of the vertical motion is reflected in the mixing ratio equation, which can be written as

$$\frac{\partial q}{\partial t} + \omega \frac{\partial q}{\partial p} + R = 0. \qquad (1)$$

Here t represents time, q the mixing ratio and R symbolically represents the remaining residual horizontal advection, forcing and damping terms.

The optimal solution of (1) that minimizes differences between model calculations and observations (Jiang and Shiao 1989) requires the minimization of the functional

$$J = \int [a^*(q - q)^2 + a^+(q - q)^2 + b^*(R - R^*)^2 + b^+(R - R^+)^2 + \lambda L]\, dp, \qquad (2)$$

where a and b are weighting factors and λ is the Lagrangian multiplier. Here * denotes model calculation while + superscripts denote observation.

The optimal mixing ratio is obtained using the Euler equation of classical variational calculus (Gelfand and Fomin 1963), yielding

$$q = \frac{(\alpha^* q^* + \alpha^+ q) + \partial(\omega^* \lambda)/\partial p}{\alpha^* + \alpha^+}, \tag{3}$$

with the Lagrangian multiplier λ

$$\frac{\partial^2(\omega^*\lambda)}{\partial p^2} - (\frac{A\alpha}{\beta})(\omega^*\lambda) = -\alpha[(\frac{\partial q^+}{\partial p} + \frac{\partial q^*}{\partial p}) + \frac{(R^+ + R^*)}{2\omega^*}] \tag{4}$$

Here $A=1/\omega^{*2}$ and $\beta>0$ can be adjusted to improve the minimization. Generally, α/β is of the order magnitude 10^{-9}. In the forcing terms on the right hand side of (4) the vertical gradient of q with respect to pressure is the dominant term, but small magnitudes of the vertical motion enhances the second term. However, from the left hand side of (4) we see that strong damping is associated with small ω , and this results in smaller gradients of $\omega^*\lambda$ which according to (3) are of lesser importance.

To produce the observed precipitable water field it is necessary to adjust the water vapor at the boundary, i.e., at the lowest pressure level, so that the vertical profile produced by equations (3) and (4) integrates to the observed total precipitable water. A mathematical shooting technique (Raymond and Kuo 1982) is used to predict this lower boundary value $q=q_0$. From (3) we find at the boundary that the vertical gradient of $\omega^*\lambda$ is given by

$$\frac{\partial(\omega^*\lambda)}{\partial p} = (\alpha^* + \alpha^+)q_0 - (\alpha^* q^* + \alpha^+ q^+). \tag{5}$$

To get the correct gradient $\omega^*\lambda$ only three or four cycles of the shooting method and corresponding solutions of (3), (4) and (5) are necessary since the shooting method converges universally and quadratically to the desired solution. An initial guess for q_0 near the average of $(\alpha^* q^* + \alpha^+ q^+)$ is reasonable. Contribution at the boundary to q_0 are distributed to the interior by the elliptic equation (4).

The vertical mixing ratio profile and the proposed modified mixing ratio are shown in Figure 1 for the case when the observed total precipitable water indicates an increase by 2.0/g. Note that the contribution from the Lagrangian multiplier is especially important in the lower atmosphere. We find that the larger the vertical motion the higher into the atmosphere the penetration of the modification. This is directly related to the magnitude of A in (4). Even though A is always positive, some comfort is taken from the knowledge that descending motion is usually small in magnitude, thus changes will usually be limited to regions closer to the surface. This appears to be a realistic response. The time tendency term can also be included in the variational process.

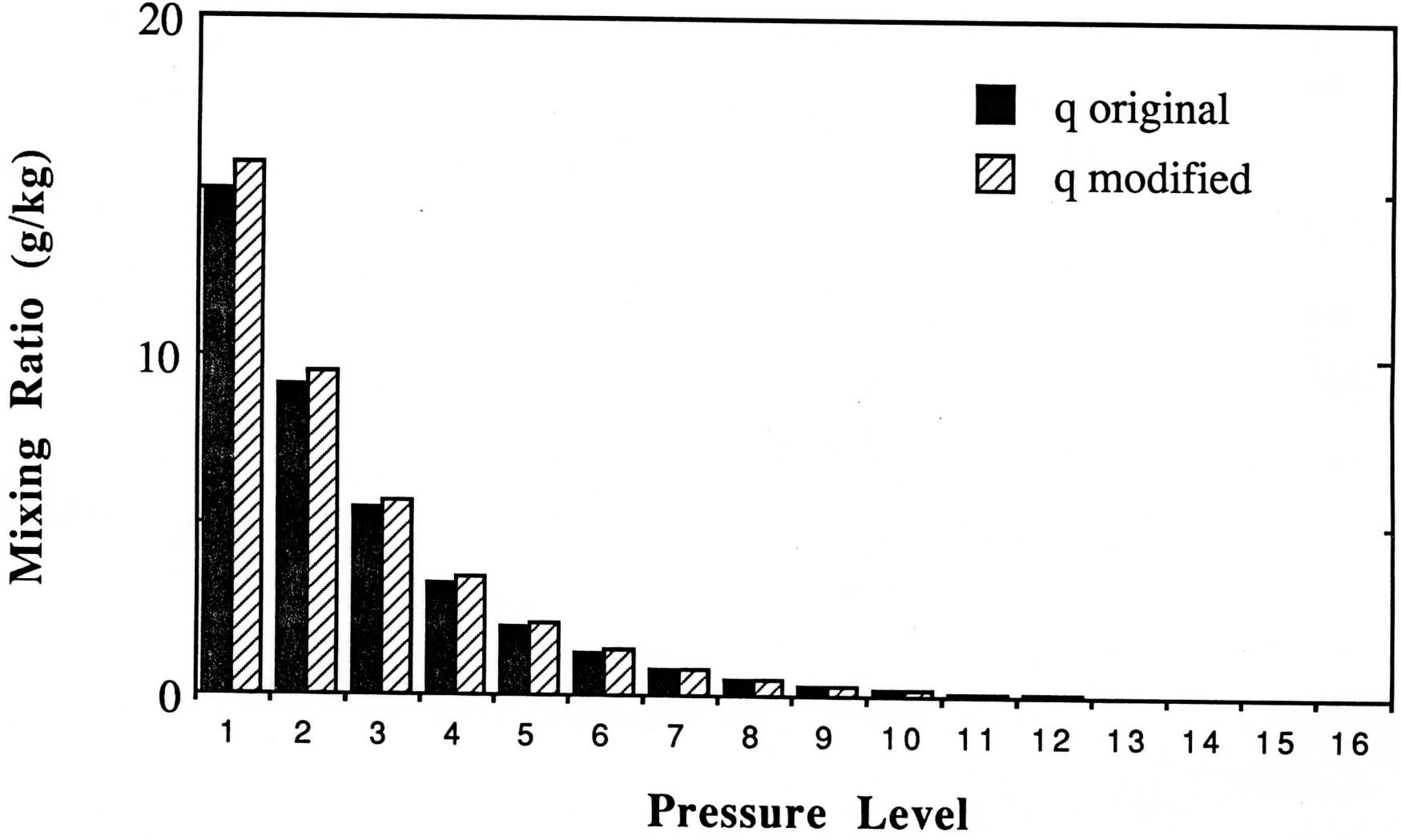
20
10
0
Mixing Ratio (g/kg)
q original
q modified
1
2
3
4
5
6
7
8
9
10
11
12
13
14
15
16
Pressure Level

Fig 2

F. Upper Tropospheric Relative Humidity from Geostationary Satellite Water Vapor Radiance Data. Contributed by Xiangqian Wu.

After modifying an algorithm developed by Schmetz and Turpeinen (1988),a quasi-operational upper tropospheric relative humidity product is being investigated at CIMSS, using geostationary satellite water vapor image data for GOES-7 and GOES-8. In a joint experiment with the European Satellite Operation Center (ESOC) the relationship between UTH and upper level winds was investigated. Figure 1 summarizes the major results of this experiment. The background is monthly mean UTH for March 1994 derived from GOES-7 (west of 92.5°W), METEOSAT-3 (92.5°W-37.5°W), and METEOSAT-5 (east of 37.5°W). The GOES-7 and METEOSAT-3 UTH were produced at CIMSS and were inter-calibrated, whereas the METEOSAT-5 UTH were produced by ESOC and were not inter-calibrated. Among other well known climate features, this image depicts the convective centers over the Amazon and Congo Basin, the storm track off the east coast of the U.S. and Canada, the strong subsidence in Central America and the Caribbean, near the Peru coast, and along the equator in Eastern Pacific Ocean. Superimposed on the UTH image are contours of upper level wind divergence, derived from a month-long average water vapor features tracked in consecutive water vapor images. The convergence/divergence correspond well to low/high value of UTH, suggesting that the water vapor in the upper troposphere is strongly related to the atmospheric dynamics.

After analyzing and verifying the March data, processing of the GOES and METEOSAT-3 UTH has been continued twice a day routinely since July 1, generating more than 50 megabytes data per day. By the end of 1994 the success rate of data archival was 80%. The plan is to collect one year's data (or as long as the satellites are available) and study the climate aspect of UTH, paying particular attention to its high spatial resolution.

With the successful launch of GOES-8, the UTH algorithm was applied to GOES-8 data. Compared with the GOES-7 UTH, the improvement in spatial resolution and signal to noise ratio are obvious, however there is a large positive bias. Further study indicates that the brightness temperatures from GOES-7 and GOES-8 agree well with each other (Figure 2a), but the forward radiative transfer models for GOES-8 and GOES-7 differ significantly for moist atmospheres (Figure 2b).

Results of this work were presented at the Eighth Conference on Atmospheric Radiation in January of 1994 (Hayden and Wu).

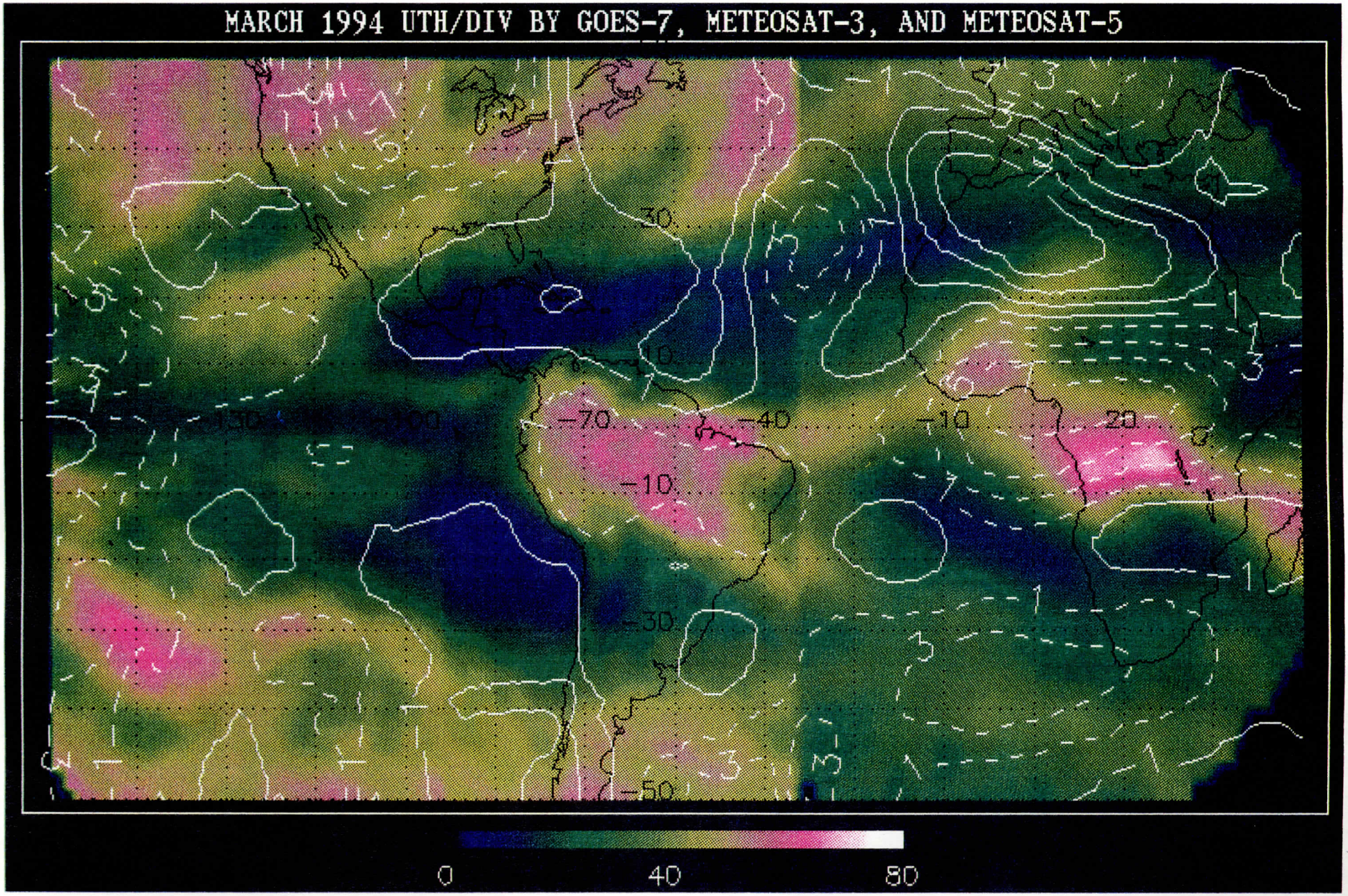
MARCH 1994 UTH/DIV BY GOES-7, METEOSAT-3, AND METEOSAT-5
-70
-40
-10
20
-10
-30
-50
0
40
80

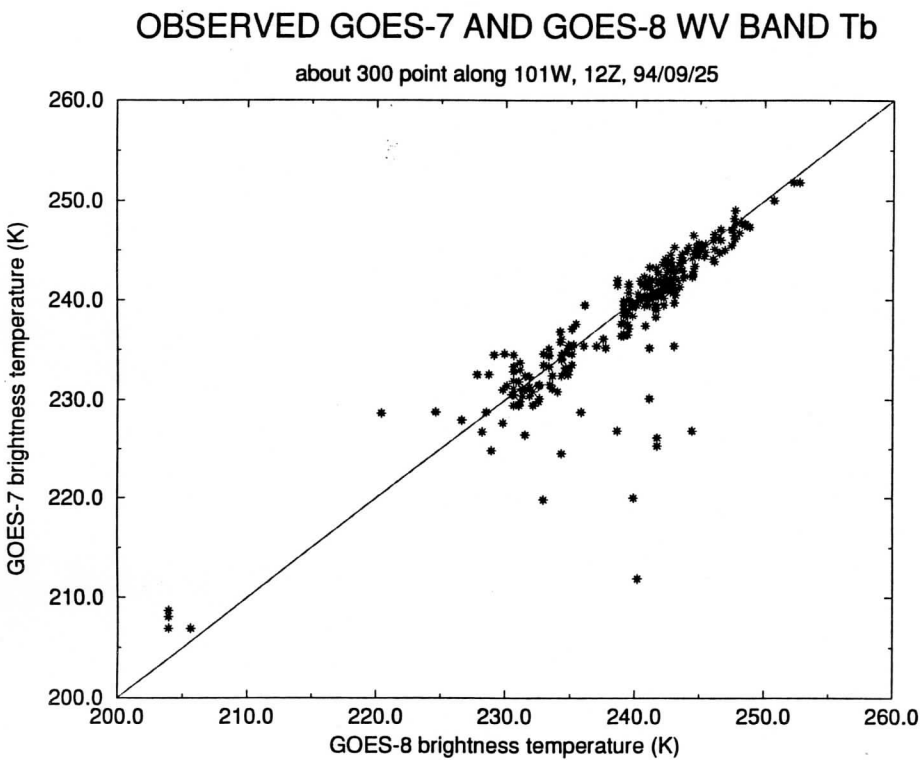
OBSERVED GOES-7 AND GOES-8 WV BAND Tb
about 300 point along 101W, 12Z, 94/09/25
GOES-7 brightness temperature (K)
GOES-8 brightness temperature (K)
260.0
250.0
240.0
230.0
220.0
210.0
200.0
200.0
210.0
220.0
230.0
240.0
250.0
260.0

Fig. 2a

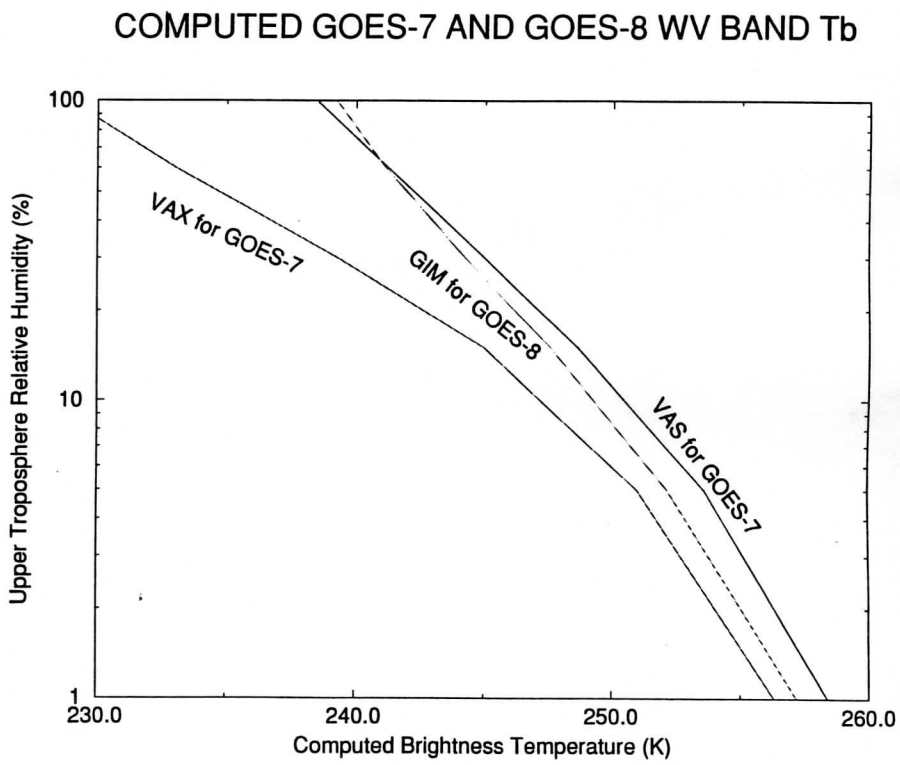
COMPUTED GOES-7 AND GOES-8 WV BAND Tb
Upper Troposphere Relative Humidity (%)
Computed Brightness Temperature (K)
VAX for GOES-7
GIM for GOES-8
VAS for GOES-7
100
10
1
230.0
240.0
250.0
260.0

Fig. 2b

G. GOES-8 derived imagery development and utilization of GALE VAS temperature/moisture retrievals. Contributed by Gary S. Wade and Robert M. Rabin.

1. Studies of moisture return to the North American Continent

A "tropical connection" of moist flow into the mid-latitudes has often been implicated from observations of cirrus cloud structure in infrared (IR) imagery. Cirrus bands emanating from the Pacific equatorial region can extend thousands of kilometers to the northeast and appear to merge with mid-latitude troughs and fronts over the U.S. The significance of these patterns in the overall moisture budget of precipitation systems is uncertain. In order to begin exploration of actual moisture transfer emanating from the equatorial Pacific, a series of total precipitable water vapor (TPWV) images derived from SSM/I were acquired from WETNET investigator Dr. Kirk Haselton (Cornell University) via the INTERNET. These SSM/I TPWV images were compared with GOES IR images and other data.

A video was produced containing time animation of 12 hourly images from the month of January 1994. A blocking ridge kept weather systems and Pacific moisture from entering the west coast of North America during most of this period. Mid-latitude systems from the central Pacific, which had inflow of high TPWV from the equator, weakened before reaching the west coast. However, channels, or "plumes", of high TPWV were occasionally observed to enter the southern Gulf of Mexico from the eastern Pacific equatorial region. The influx of moisture traversed southern Mexico from south to north near the Gulf of Tehuantepec and the Bay of Campeche. During the month of study, penetration of high TPWV into the southern Gulf was preceded by increasing TPWV well to the southwest in the eastern Pacific. Extension of this analysis to more diverse synoptic conditions is required.

This videotape was presented and discussed by Dr. R. M. Rabin (NOAA/NSSL scientist at CIMSS) at an AOS/SSEC colloquium entitled: "SSM/I Measurement of Precipitable Water" on 14 March 1994.

[See Figure 1, for an example of the composite SSM/I derived TPWV image (on the left) and the GOES IR image (on the right) for 0000 UTC on 15 January 1994, as assembled on the videotape. Note the high moisture regions: one extending westward from northwestern South America (indicating the Intertropical Convergence Zone) and two others both extending northeastward, one from south of the West Coast of the U.S. and the other across the Greater Antilles (both plumes being associated with mid-latitude frontal systems).]

2. Comparison of moisture fields derived from satellite

For assessment of the quality of the instruments on the newly launched GOES-8 satellite (April 1994), daily composites of SSM/I derived product imagery (DPI) of total precipitable water vapor (TPWV) were acquired in real-time from NOAA's MIDAS (Meteorological Interactive Data Access System) computer and archived to tape. These SSM/I DPI, created from a statistical formulation (of radiances

regressed with radiosonde data), provided an independent source of comparison for both GOES-7 and GOES-8 DPI over water backgrounds. With better horizontal resolution and signal to noise characteristics, the GOES-8 Imager DPI, generated with a physical retrieval formulation, was a dramatically improved product compared to the GOES-7 VAS MSI (Multi-Spectral Image) DPI. Comparison with the SSM/I generally confirmed the patterns and features seen with the GOES-8 DPI, but which were often only suggested by the GOES-7 DPI. The emphasis on the impact of moisture from the Gulf of Mexico on the weather of the central US has continued from earlier satellite work with the GUFMEX experiment in 1988 and later.

[See Figure 2, for a sample comparison of GOES-7 (left), GOES-8 (center), and SSM/I (right) TPWV DPI from 23 November 1994 near 0000 (top) and 12 (bottom) UTC. Note how the secondary dry pockets extending into the southwestern Gulf of Mexico are depicted in each of the DPI near 0000 UTC.]

3. Assessment of assimilation of satellite retrievals from GALE

Following previous provision to Dr. F. Ruggiero (Naval Research Lab) of 23 data sets of atmospheric profiles from the VAS Sounder during the Genesis of Atlantic Lows Experiment (GALE) Intensive Observing Period (IOP) from 23 to 28 January 1986, an additional request was entertained to provide a number of infrared images from the same period. A search within SSEC showed that only a limited number of GOES imagery remained in an easily accessible format on tape. (The original GOES data still reside within the national GOES archive, housed at SSEC; however, retrieval of imagery from that source would involve considerable expense). A workable selection of the available imagery was restored to the McIDAS mainframe which was then accessed by Ruggiero from a McIDAS workstation at North Carolina State University, where he continues to evaluate his assimilation experiment from the GALE IOP data set, including the impact of the VAS retrieval profiles.

4. Surface skin temperature fields as monitored from geostationary satellites

GOES-8 Imager radiances have been used to generate derived product imagery (DPI) of surface skin temperatures, incorporating adjustments to window channel values due to attenuation by atmospheric moisture as determined in the retrieval processing. With frequent imaging available from a geostationary platform (on the scale of an hour) at nominal 4 km horizontal resolution, the GOES-8 Imager skin temperature DPI can be used to assemble a more complete depiction of surface temperature over a given period of time as obscuring clouds move in and out of the area of interest. Both maximum and minimum values can be determined, with possible local scale applications ranging from forecasting of afternoon convection (at "hot spots") to delineation of early morning "cold pools"; slowly varying fields of water surface temperature (or SST, sea surface temperature) are also included.

[See Figure 3, for an example of time compositing four skin temperature DPI from the GOES-8 Imager on 31 January/1 February 1995. The four images on the left and in the center show the skin

temperature progression at six hour intervals from 2245 UTC on the 31st to 1645 UTC on the 1st. The images on the right show the maximum (top) and minimum (bottom) values from the four just described. Note how complete and steady are the Gulf of Mexico SST fields as shown in both of the composites, with the warm Loop Current evident in the southeastern Gulf. For better determination of land skin temperature extremes, higher temporal resolution observations from GOES-8 would be used.]

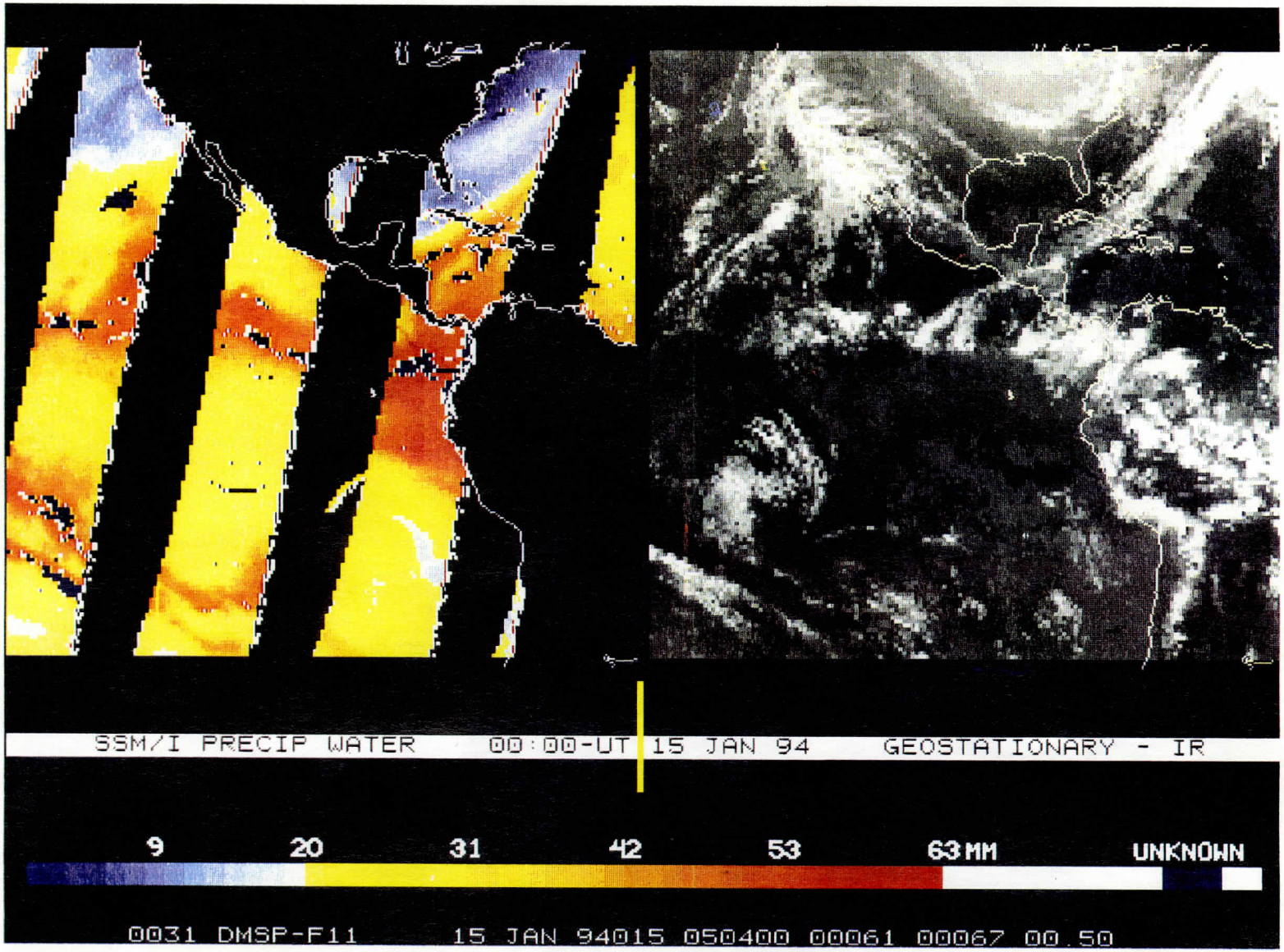
SSM/I PRECIP WATER 00:00-UT 15 JAN 94 GEOSTATIONARY - IR
9 20 31 42 53 63 MM UNKNOWN
0031 DMSP-F11 15 JAN 94015 050400 00061 00067 00.50

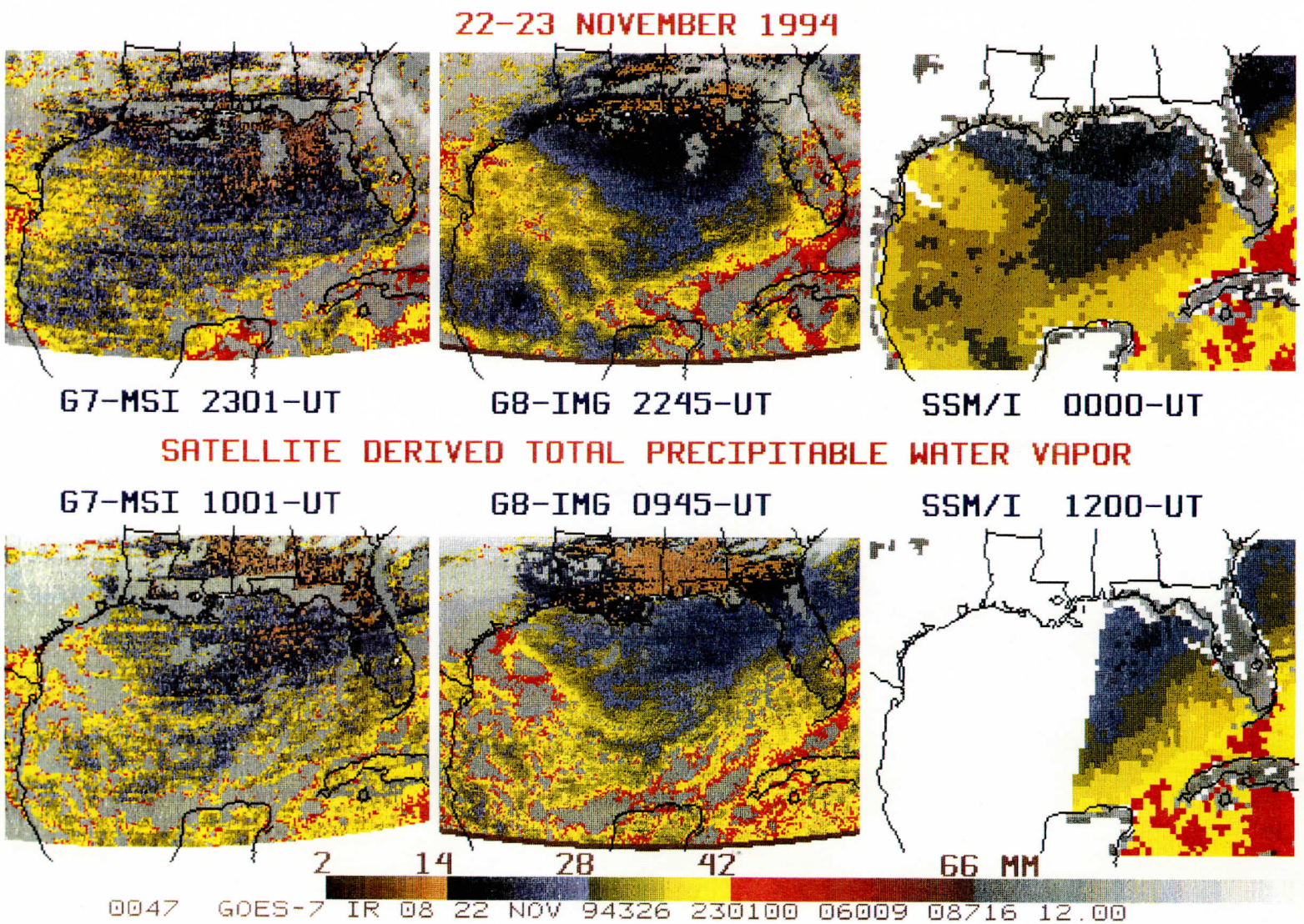
22-23 NOVEMBER 1994
G7-MSI 2301-UT
G8-IMG 2245-UT
SSM/I 0000-UT
SATELLITE DERIVED TOTAL PRECIPITABLE WATER VAPOR
G7-MSI 1001-UT
G8-IMG 0945-UT
SSM/I 1200-UT
2
14
28
42
66 MM
0047 GOES-7 IR 08 22 NOV 94326 230100 06009 08716 12.00

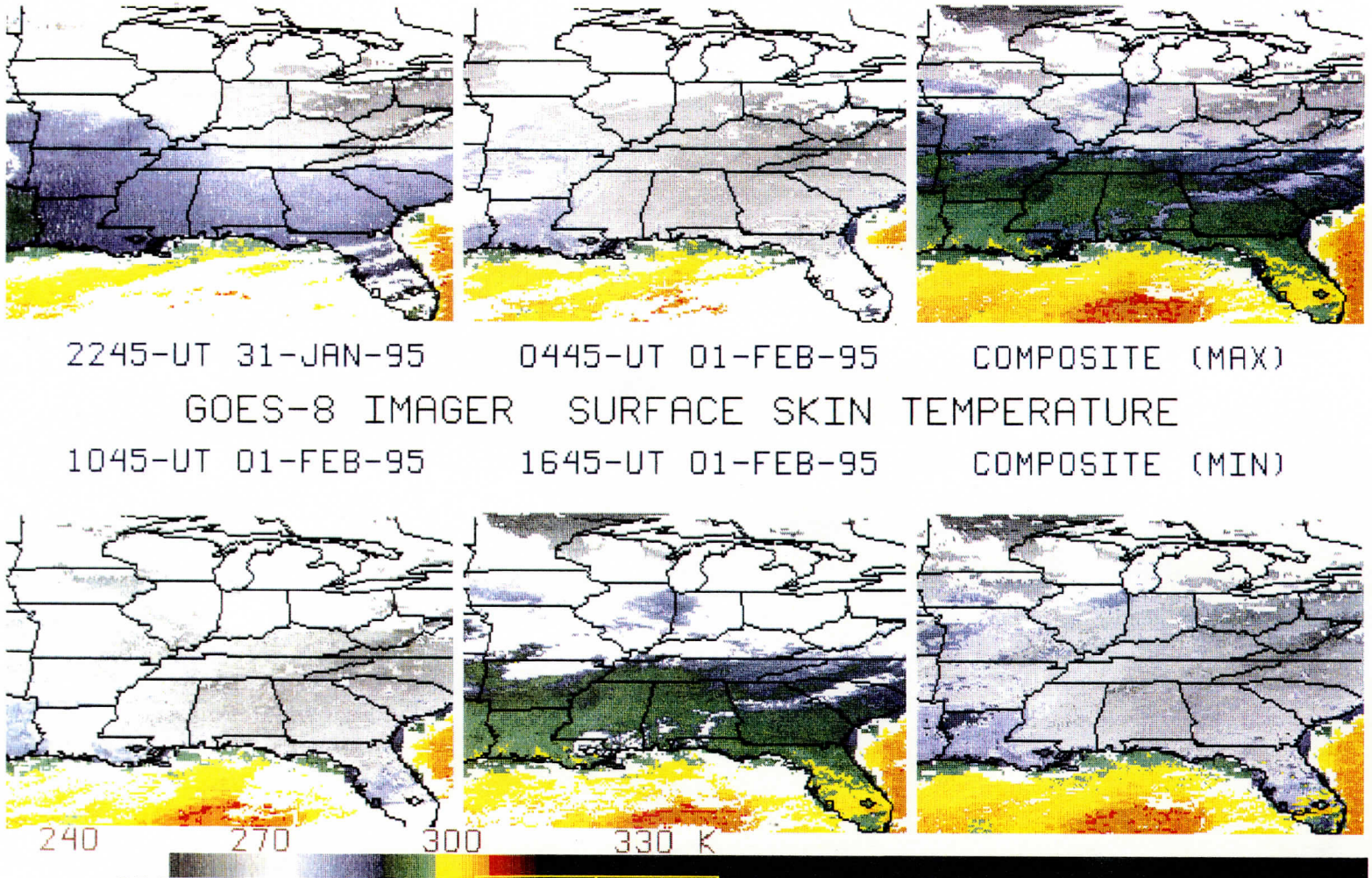
2245-UT 31-JAN-95
0445-UT 01-FEB-95
COMPOSITE (MAX)
GOES-8 IMAGER SURFACE SKIN TEMPERATURE
1045-UT 01-FEB-95
1645-UT 01-FEB-95
COMPOSITE (MIN)
240
270
300
330 K
0067 G-8 IMG 08 31 JAN 95031 224500 02989 13908 12.00

H. Development of a Microburst Risk Image Product from Satellite Sounder Data. Contributed by James P. Nelson and Gary P. Ellrod.

In terms of input data used to derive microburst risk predictors, it has been shown that VAS (VISSR Atmospheric Sounder) retrievals of temperature and moisture are useful for diagnosing the pre-convective mesoscale state of the atmosphere, given that one is using parameters that minimize the well-known weakness of satellite retrievals to resolve fine vertical atmosphere structure. Satellite retrievals, especially for the recently launched GOES-8, are much more timely than the twice-daily radiosondes, and they represent actual atmospheric conditions, as opposed to the forecast conditions output by numerical models. Therefore, these retrievals should be useful for monitoring the continually-changing state of the atmosphere, an important quality needed for microburst prediction.

There are some things to be kept in mind when using satellite retrievals for deriving microburst risk predictors, however. Zehr et al. (1988) noted a persistent bias towards larger lapse rates in the 700-400 hPA later, which will tend to lead to overestimates of Convective Available Potential Energy (CAPE), which is used to identify regions where microbursts may potentially occur. This is a concern, but the satellite retrievals derived from GOES-8 are expected to be superior to those from GOES-7 (Menzel and Purdom 1994). This will hopefully lead to reductions in some of the biases and therefore more accurate microburst risk imagery. Moreover, microburst risk imagery is intended only to alert forecasters to regions of relative microburst risk, not of absolute microburst occurrence, and the forecaster should be able to further assess the situation once forewarned by using other supplementary data.

Displaying the regions of microburst risk in the form of an image that is color-enhanced has two distinct advantages. First, a color image will tend to visually lead a forecaster to high-risk areas more quickly. The second advantage is that a well-conceived image can show information in a more orderly and easier-to-interpret fashion than a graphical analysis.

All work was performed on one of the Man-computer Interactive Data Access Systems (McIDAS) housed at the NOAA Science Center in Camp Springs, MD. For data from a given time, grids of various predictor quantities (Lifted Index, 850-700 hPA lapse rate, 500 hPA relative humidity, vertical differences in equivalent potential temperature from the surface to 700 hPA, time changes, and time changes of those vertical differences) were created for a specified geographic region. Following this, the predictor grids to be used in generating the microburst risk image were chosen. For a given predictor grid, each grid point was changed from the predictor quantity to either a 1 or a 0, depending on whether the predictor met a pre-assigned criterion for microburst risk. Then, the 1 to N predictor grids were added together to create an output microburst risk grid. At this point in the process, each grid point within the microburst risk grid contained a value ranging from 0 (no positive microburst risks) to N (N positive microburst risks). Following this, the risk grid point values were reassigned to fit within a range of 0-254 for subsequent image generation and color enhancement. The actual reassigned values were determined by how many

predictors were used to produce the microburst risk grid, the reassigned grid point values were as follows: 0 (no affirmative microburst conditions), 85,170, or 254 (3 affirmative microburst conditions).

After a given microburst risk grid was built, an image was created from the grid. An enhancement curve was then applied to the image, resulting in a color-coded image that readily displayed areas where 0, 1, 2, or all 3 microburst predictors were positive. In all cases, the color red was used to highlight areas where all predictors were true.

This technique is currently applied to GOES-7 temperature/moisture retrievals. With the recent launch of GOES-8 and in the current operation mode, hourly profiles of temperature and moisture will be produced. In addition to the more timely retrievals possible with this new satellite, it is expected the retrievals themselves will be of a higher quality than the same from GOES-7. This should reduce the retrieval biases mentioned earlier and therefore should allow for more accurate microburst risk imagery. With this in mind, future plans include investigation of antecedent microburst conditions using GOES-8 retrievals. Further work will focus on utilizing other potential predictors and combinations of predictors in microburst risk imagery, and on attempting to define imagery specific to either wet microburst or dry microburst situations. Software will also be developed that will allow operational production of the imagery.

I. **Development of a Gridded Cloud Product from GOES-8 Radiance Data.** Contributed by Anthony J. Schreiner and Christopher M. Hayden.

Introduction

In support of the Global Energy and Water Cycle Experiment (GEWEX) Continental International Project (GCIP) cloud products augmenting the Automated Surface Observing System (ASOS) have been developed utilizing radiance information from the GOES-8 infrared sounder. Being that the ASOS is only limited to a description of cloud cover up to 12,000 ft., application of the CO_2 absorbing bands on the GOES-8 along with the CO_2 absorption technique (Menzel et al. 1983) for defining mid and upper level cloud parameters, make the two observing systems complementary.

The goal of this work is to develop a system to routinely calculate cloud height and effective amount on an hourly basis over the continental U.S. (CONUS) on a lat./lon. grid at 0.5 degree interval. The quantities to be calculated are average cloud top pressure, effective cloud amount, skin temperature, and a quality control flag indicating whether the grid box was clear or cloudy. No products are generated from areas where the satellite local zenith angle exceeds 60°.

Background

There are primarily two major steps in the generation of the satellite-derived product. The first is the cloud identification step (CIS) and the second is the cloud calculation step (CCS). The technique to accomplish the first step is the same cloud clearing process used in the temperature/moisture retrieval algorithm (an incredibly complicated and continuously changing process). Input used in the cloud clearing process is the radiance of the window channel and the first guess skin temperature (or sea surface temperature). Within a 5 x 5 box the long wave window measurements are compared to the warmest and tentatively accepted if they are not colder than a pre-determined threshold. Each field of view (fov), including the warmest, must also pass a battery of radiance tests which seek to identify thin cirrus, low level stratus, excessive reflected sunlight, and variable surface emissivity. There is also a check for consistent topography, and a flag can be given if it varies dramatically. Each fov emerges with a flag of clear, possibly clear, or cloudy (Hayden and Schmit, 1994). The first and the last flags are accepted, but the middle definition requires some additional testing once a cloud top pressure and effective amount are determined in the CCS.

The purpose of using the cloud clearing technique (CCT) is to identify whether a given fov is clear or cloudy. If it is found to be clear, the processing continues to the next fov. The processing method works on 5 x 5 fov boxes, as it generates cloud information for an entire sounding image. When a cloudy fov is found, it is flagged as such. The CCT then continues to the next fov within a 5 x 5 box until all fov's are either flagged cloudy or clear. Then the CO_2 absorption technique (CAT) determines the level and effective amount of the cloud. For each box an average cloud top pressure and effective amount is

determined in addition to the cloud parameter calculations for each fov. The individual calculations are used in generating a cloud top pressure/effective amount image.

The CAT uses radiation measurements in three spectral channels in the CO_2 absorption band (14.05, 13.65, and 13.38μm) and in the infrared window at 11.03μm. The three channels in the CO_2 absorption band differentiate cloud altitudes and the long wave infrared window channel identifies effective cloud amount in the GOES-8 FOV. The CAT method cannot be used when clear and cloudy sky radiance differences fall within instrument noise level. This occurs for very thin clouds (such as high thin cirrus) or for low warm clouds. In these situations, a cloud-top pressure is calculated directly from comparison of observed infrared window channel brightness temperature and an in situ temperature profile; the cloud is assumed to be opaque with an effective cloud amount of one (Schreiner et al. 1993).

Results

The current format of the product is available in both a gridded format (Figure 1) and an image format (Figure 2). It is routinely being produced on a RISC 6000 computer at UW-CIMSS. Figure 3 demonstrates an example of the evolution of cloud top pressure over the United States over the course of one 24 period for 20 April 1995.

Summary and Future Work

Through the use of GOES-8 radiance information a scheme to generate images or a gridded product of cloud top pressure and effective amount has been developed. The scheme is currently generating images or gridded data every three hours. It is our intention to increase the frequency to an hourly product. Future applications would replace the current site specific satellite-derived cloud product used to supplement the ASOS. The primary advantage would be to allow the nowcaster/forecaster the opportunity to get a contiguous picture of cloud top pressure and effective cloud amount over the continental U.S. rather than a sub-sample picture as depicted in the current site dependent product.

Figure Captions

Figure 1. Gridded analysis of Effective Cloud Amount (left) in per-cent for 20 April 1995 2346 UTC and Derived Cloud Top Pressure (right) in hPa. from GOES-8.

Figure2. Derived image of GOES-8 Cloud Top Pressure in hPa. for 20 April 1995 2346 UTC.

Figure 3. Four panel of GOES-8 Derived Cloud Top Pressure for 20 April 1995 at 0246 UTC (upper left), 0846 UTC (upper right), 1746 UTC (lower left), and 2346 UTC (lower right).

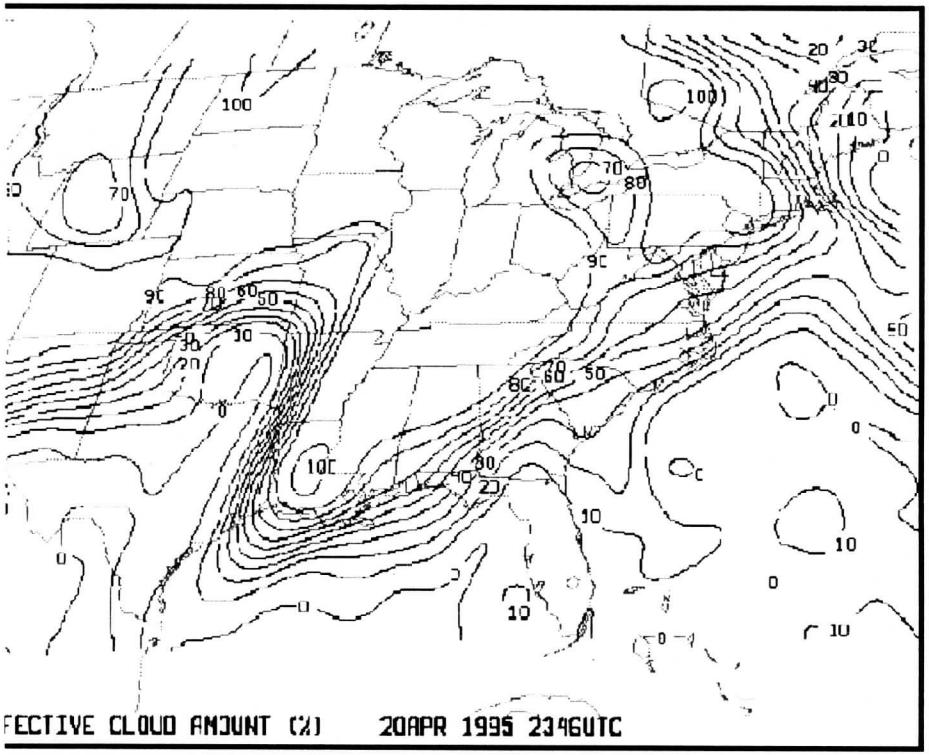
FECTIVE CLOUD AMOUNT (%) 20APR 1995 2346UTC

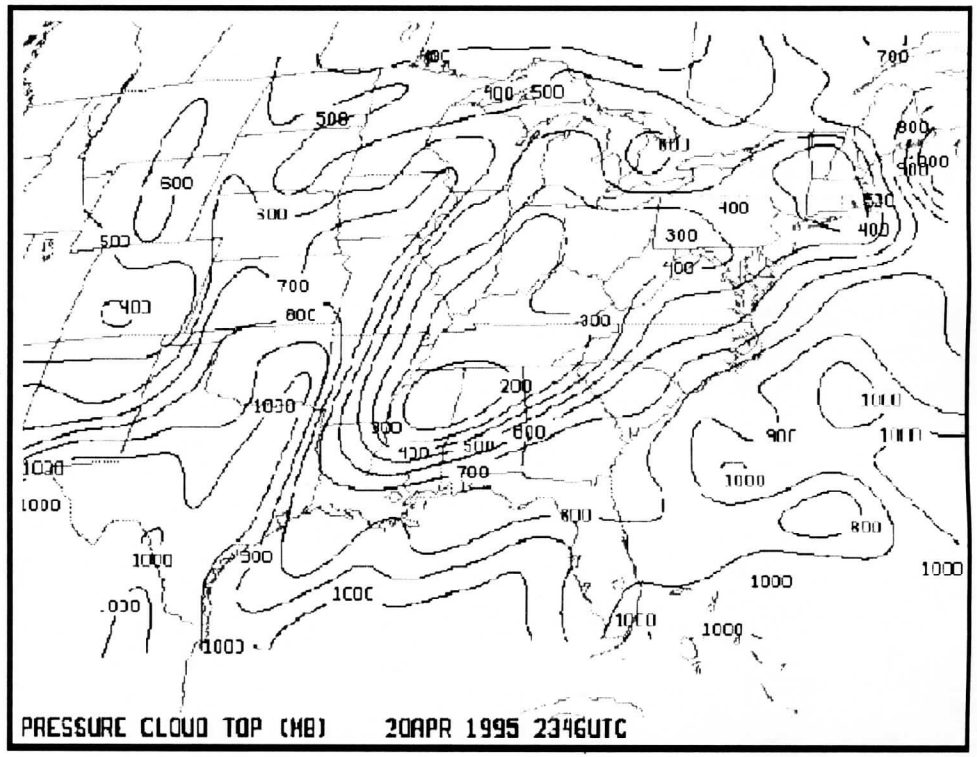
PRESSURE CLOUD TOP (MB) 20APR 1995 2346UTC

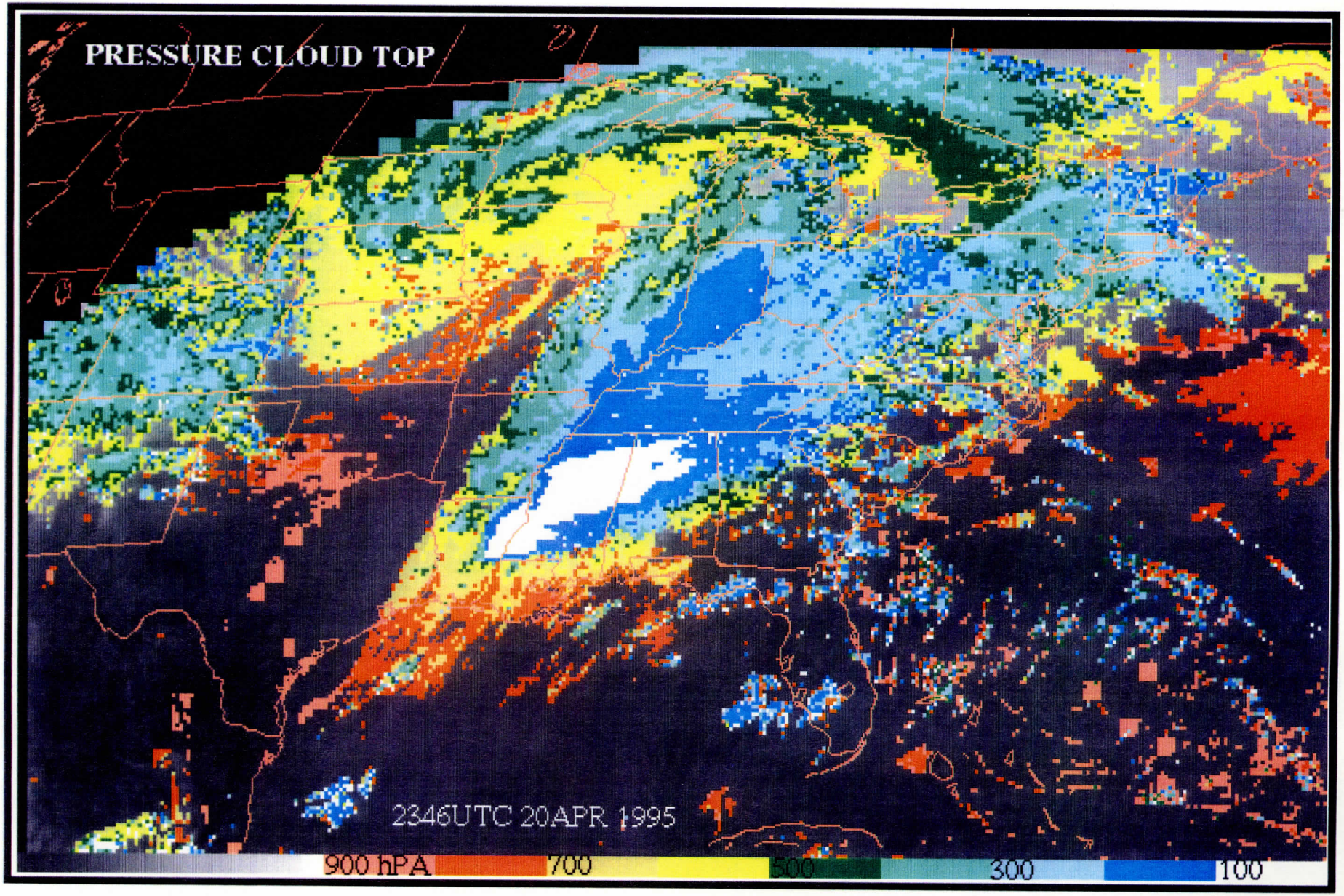
PRESSURE CLOUD TOP
2346UTC 20APR 1995
900 hPA
700
500
300
100

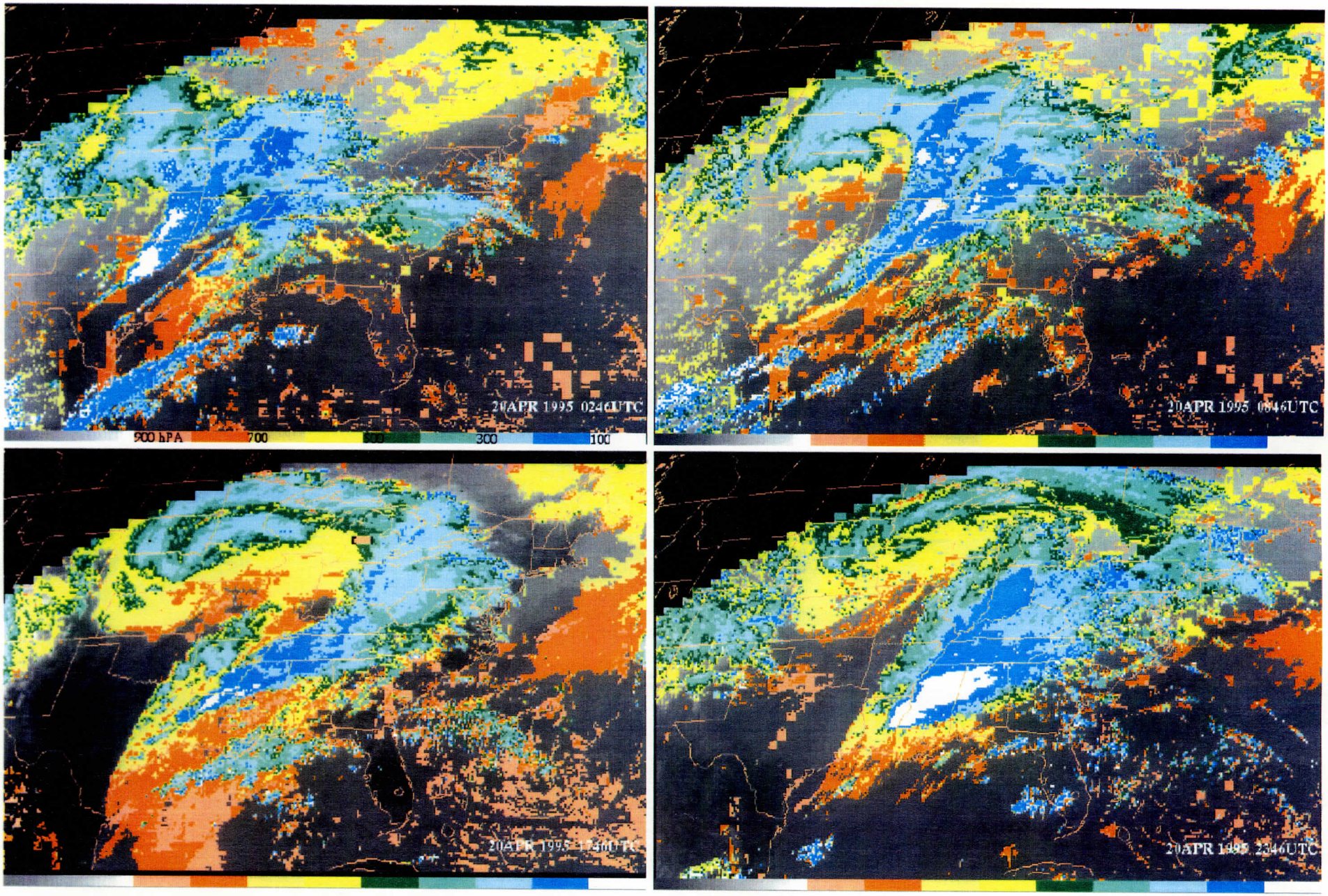

GOES–8 SOUNDER PRESSURE CLOUD TOP

UW - CIMSS

III. PERSONNEL AND EQUIPMENT

Personnel

	LABOR (%)	COMPUTER (%)
SSEC		
James P. Nelson	100	100
Daphne Olander	100	100
William H. Raymond	100	75
Anthony J. Schreiner	20	20
William L. Smith	5	5
Mark Whipple	20	20
Xiangqian Wu	80	80
Xiaohua Wu	100	100
NESDIS		
Robert M. Aune		100
Geary M. Callan		100
Christopher M. Hayden		50
Leroy D. Herman		100
Frederick W. Nagle		50
Gary S. Wade		33
NSSL		
Robert M. Rabin		10
Visiting Scientist		

The numbers underneath the column "LABOR" represent the percentage of their labor time which was charged to this project. The percentages below the column headed by "COMPUTER" indicate the amount of computer time which the scientists charged to this contract. Both percentages are based on one year being equivalent t 100%. NESDIS employees' labor is provided from funds outside of this contract.

Equipment

None

IV. SUMMARY

The support from this contract has been important in providing the programmers, research scientists, and support staff the opportunity to perform a wide variety of research within the CIMSS organization. Many of the areas of research which were discussed in Section II are ongoing topics.

V. REFERENCES

Aune, R. M., 1994: Improved precipitation predictions using total precipitable water from VAS. *Preprint, Tenth Conference on Numerical Weather Prediction, Amer. Meteor. Soc.,* Portland, OR, 18-22 July, 1994, pp. 192-194.

Gelfand, I. M., 1963: Calculus of Variations. Prentice-Hall, Inc., New Jersey, 232pp.

Hayden, C.M and R.J. Purser, 1994: Recursive filter objective analysis of meteorological fields, applications to NESDIS Operational Processing. To be published in the *Jour. Appl. Meteor.*, **34**,3-15.

Hayden, C.M. and Xangquin Wu, 1994: Upper tropospheric relative humidity estimates fro GOES. *Preprint Volume, Eighth Conference on Atmospheric Radiance*, Jan 27-28, Nashville, TN, AMS, 58-60.

Herman, L.D., 1993: High frequency satellite cloud motion at high latitudes. *Eighth Symposium on Meteorological Observations and Instrumentation*, Anaheim, CA, Jan. 17-22, 1993.

Herman, L.D. and F.W. Nagle, 1994: A comparison of POES satellite derived winds techniques in the arctic at CIMSS. *Preprint volume, Seventh Conference on Satellite meteorology and Oceanography*, Monterey, CA, June 6-10, 1994.

Jiang, H-M., and C-H. Shiao, 1989: Numerical experiments of data assimilation using the shallow-water equation model. Papers in *Meteorological Research*, **12**, 33-57.

Menzel, W.P. and J.F.W. Purdom, 1994: Introducing GOES-I: The first of a new generation of geostationary operational environmental satellites. *Bull. Amer. Meteor. Soc.*, **75**, 757-781.

Orlanski, I., 1981: The quasi-hydrostatic approximation. *J. Atmos. Sci.*, **38**, 572-582.

Pauley, P.M. and X. Wu, 1994: Reply for comments on "The theoretical, discrete and actual response of the Barnes objective analysis scheme for one- and two-dimensional fields". *Mon. Wea. Rev.*, Vol. **122**, No. 2, 399-401.

Rabin, R.M., L.A. McMurdie, C.M. Hayden, and G.S. Wade, 1993: Evaluation of the atmospheric water budget following an intense cold air outbreak over the Gulf of Mexico-Application of a regional forecast model and SSM/I observations. *Jour. Appl. Meteor.*, **32**, 3-16.

Raymond, W.H., 1993: Moist wind relationships. *Mon. Wea. Rev.*, **121**, 1992-2003.

Raymond, W.H., 1993: Numerical filters and their applicability. Submitted to *Mon. Wea. Rev.*

Raymond, W.H., 1993: Rotationally induced circulations: Equatorial meridional flows. Submitted to *J. Atmos. Sci.*

Raymond, W.H., 1994: Diffusion and numerical filters. *Mon. Wea. Rev.*, **122**, 757-761.

Raymond, W. H., and H. L. Kuo, 1982: Simulation of laboratory vortex flow by axisymmetric similarity solutions. *Tellus*, **34**, 588-600.

Zehr, R.M., J.F.W. Purdom, J.F. Weaver, and R.N. Green, 1988: Use of VAS data to diagnose the mesoscale environment of convective storms. *Wea. Forecasting*, **3**, 33-49.